

# Segmentation of High-resolution InSAR Data of Tropical Forest using Fourier Parameterised Deformable Models.<sup>1</sup>

Chris Varekamp and Dirk H. Hoekman

Dept. of Environmental Sciences, Nieuwe Kanaal 11, 6709 PA Wageningen, The Netherlands

tel:+31-317-482765, fax:+31-317-484885,

email: chris.varekamp@users.whh.wau.nl, dirk.hoekman@users.whh.wau.nl

## Abstract

Currently, tree maps are produced from field measurements that are time consuming and expensive. Application of existing techniques based on aerial photography is often hindered by cloud cover. This has initiated research into the segmentation of high resolution airborne interferometric Synthetic Aperture Radar (SAR) data for deriving tree maps. A robust algorithm is constructed to optimally position closed boundaries. The boundary of a tree crown will be best approximated when at all points on the boundary, the  $z$ -coordinate image gradient is maximum, and directed inwards orthogonal to the boundary. This property can be expressed as the result of a line integral along the boundary. Boundaries with a large value for the line integral are likely to be tree crowns. This paper focusses on the search procedure and on illustrating how smoothing can be used to prevent the search to become trapped in a local optimum. The final crown detection stage is not described in this paper but could be based on the gradient and implemented using the above described value for the line integral. Results of this paper indicate that a Fourier parameterization with only three harmonics (nine parameters) can describe the shape variation in the 2D crown projection in sufficient detail. Current ground data sets are not suitable for obtaining detection statistics such as the percentage of tree crowns detected and the number of false alarms. Better ground data sets will be needed to evaluate algorithm performance for real tree mapping situations.

## 1 Introduction

To enforce national legislation for sustainable forest management or to verify implementation of guidelines for sustainable forest management as proposed by the International Tropical Timber Organization (ITTO), information on terrain, forest and tree characteristics is needed. Tree identification is important for detecting illegal cutting. Cutting guidelines are often based on a combination of tree stem diameter and species. Trees with a large stem diameter are economically important and only a certain number may be harvested each year. These trees are either high or have a large crown. The tree crown 3D position and size can thus be important indicators for trees with a large stem diameter.

In this paper we describe an algorithm for estimating the 3D position and crown size of large trees. At C-band, the backscattered signal originates mostly from tree

crowns in the upper canopy of the forest. The SAR imaging process projects the 3D scattering tree crown volume into 2D cylindrical zero-Doppler radar coordinates (Bamler and Hartl, 1998). For most tree crown shapes, this 2D projection will resemble well a circular boundary. Detection of this 2D projection is seen as a segmentation problem. A model based segmentation is used since the data exhibit much noise. Many possible parameterizations have been reported for geometric shapes (Kass et. al., 1988, Staib and Duncan 1992, Cootes et. al. 1995). In this paper we use an elliptic Fourier parameterization for the tree crown boundary (Staib and Duncan 1992, Chakraborty and Duncan 1999). This parameterization can represent a tree crown well with a small number of parameters. To our knowledge the technique has been applied to heart and brain images using magnetic resonance images (Staib and Duncan 1992) but not yet to interferometric phase difference images.

The contributions of this paper are twofold. Firstly, it is shown that estimation of tree crown 3D position can be successful using a circle or a smooth Fourier parameterization for the 2D projection of the 3D tree crown. Secondly, the interferometric coherence magnitude is used explicitly in the estimation procedure by giving pixels with a high coherence more weight than pixels with a low coherence. The physics of SAR imaging is also used explicitly: Deterministic displacements are corrected for using the Van Cittert-Zernike Theorem and the noise model is based on stochastic knowledge of electromagnetic scattering.

## 2 Experiment description

### 2.1 InSAR data

High-resolution (100 MHz) C-band interferometric SAR data were acquired by the Dornier-SAR system during the Indonesian Radar Experiment 1996 (INDREX '96) in Indonesia (Faller 1998, Hoekman and Varekamp 1998, Wooding et. al. 1999). Figure 1 shows 4-look slant range images of the intensity, the interferometric  $z$ -coordinate, and the coherence for track KAL.17A. Each image is 120 lines by 160 samples, and the pixel spacing is 1.249 m in range direction and 1.365 m in azimuth direction. Large tree crowns appear bright on the intensity image and on the  $z$ -coordinate image, but dark on the coherence image.

<sup>1</sup> Proc. INDREX Final results workshop, ESTEC 9 Nov. 1999 & Jakarta 30 Nov. 1999; ESA SP-489, Nov. 2000, p 57-62



Figure 1. Subset of 4-look slant range radar data: (a) intensity, (b) interferometric z-coordinate, and (c) coherence magnitude for track KAL.17A.

## 2.2 Ground truth

Ground measurements of crown positions and crown dimensions were collected in Kalimantan in August 1998. The distance between a trees trunk centre and its crown projection were measured. Ground measurements were then transferred into radar coordinates using one tree as a tie points.

## 3 Parameterisation of the 2D crown projection

Consider the radar image as a rectangular coordinate system with range coordinate  $r$  and azimuth coordinate  $x$ . The elliptic Fourier representation of a closed curve  $v(t)=(r(t),x(t))^T$  in this coordinate system is given by

$$v(t) = \begin{bmatrix} a_0 \\ c_0 \end{bmatrix} + \sum_{k=1}^{K-1} \begin{bmatrix} a_k & b_k \\ c_k & d_k \end{bmatrix} \begin{bmatrix} \cos kt \\ \sin kt \end{bmatrix} \quad (1)$$

where  $t$  varies from 0 to  $2\pi$  and  $K$  is the number of harmonics. The curve is completely described with  $4K-2$  parameters, with  $K \geq 2$ . The coefficients  $a_0$  and  $c_0$  determine the overall translation of the shape. Each term in the summation is the parametric form for an ellipse. Limiting  $K$  makes the curve smooth by excluding functions with higher frequency variation. The number of harmonics used in a particular segmentation depends on the required detail in the boundary description and the image noise level. The question arises how many harmonics are needed to represent a tree crown. This was investigated using stereo aerial photographs. The parameters in (1) were derived from digitized boundaries using the Fourier transform relations:

$$\begin{aligned} a_0 &= \frac{1}{2\pi} \int_0^{2\pi} r(t) dt & c_0 &= \frac{1}{2\pi} \int_0^{2\pi} x(t) dt \\ a_k &= \frac{1}{\pi} \int_0^{2\pi} r(t) \cos ktdt & b_k &= \frac{1}{\pi} \int_0^{2\pi} r(t) \sin ktdt \\ c_k &= \frac{1}{\pi} \int_0^{2\pi} x(t) \cos ktdt & d_k &= \frac{1}{\pi} \int_0^{2\pi} x(t) \sin ktdt \end{aligned} \quad (2)$$

Figure 2 illustrates the effect of  $K$  on the boundary shape. Three harmonics ( $K=3$ ) seem sufficient considering that a pixel dimension is roughly one tenth the dimension of the boundaries shown in figure 2. We therefore decide to use  $K=3$  harmonics.

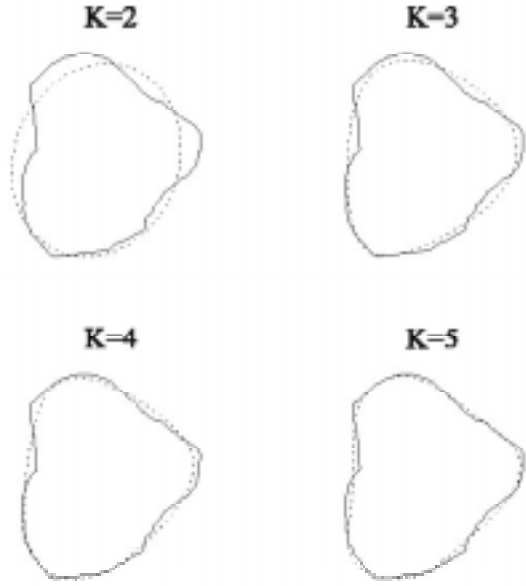


Figure 2. Effect of  $K$  on the boundary shape. The solid line is the original boundary derived from stereo aerial photographs. The dotted lines are reconstructions using only  $K$  harmonics.

The parameter representation of equation (1) does not allow a straightforward geometric interpretation. This would be useful to be able to specify geometric constraints on boundary size and shape in the next section. A parameter interpretation in terms of ellipses is possible. For two harmonics we can form the following parameter vector describing two ellipses in terms of relative ellipse parameters (Staib and Duncan 1992)

$$p = (a_0, c_0, A_1, B_1, \theta_1, A_2, B_2, \theta_2, \psi_2)^T \quad (3)$$

The ellipse semi-axis are  $A$  and  $B$ . The subscript indicates the ellipse (harmonic) number. Parameter  $\theta_1$  determines the absolute overall rotation of the shape. It is the absolute ellipse rotation angle  $(-\pi/2, \pi/2)$  from the  $r$ -axis to the major semi-axis  $A_1$  of the first ellipse. Parameter  $\theta_2$  is the relative rotation  $(-\pi, \pi)$  of the first ellipse major semi-axis  $A_1$  to the second ellipse major axis  $A_2$ . Then there is one remaining parameter: phase shift  $\psi_2$   $(-\pi, \pi)$ . This is the relative phase from the major semi-axis of the first ellipse to the major axis of the second ellipse. In conclusion, the shape ellipse semi-axis parameters  $A_1, B_1, A_2, B_2$  and the overall rotation  $\theta_1$  are absolute quantities whereas all other parameters are relative to the preceding harmonic. This makes it possible to isolate an overall shape rotation  $\theta_1$  and to remove an overall phase shift  $\psi_1$ . The relative ellipse parameters in equation (3) are related to the Fourier expansion in equation (1) through simple combinations of trigonometric functions. We do not give their relations here but refer to the treatment by Staib and Duncan (1992).

The Fourier boundary can be non-smooth when the derivatives  $r'(t)$  and  $x'(t)$  are simultaneously zero (Edwards and Penney, 1994). We expect that crown boundaries are smooth in general and therefore do not allow non-smooth boundaries. Boundaries are constrained by a maximum curvature of 0.5 (A circle with radius of 2 m has curvature of 0.5).

## 4 Segmentation

### 4.1 Use of gradient information

Segmentation is based on the gradient of the filtered interferometric  $z$ -coordinate. Filtering is done with a circular window shape. The filtering operation takes into account the uncertainty of the pixel position as indicated by the interferometric coherence magnitude  $|\rho|$ . The filtered  $z$ -coordinate of the centre pixel is calculated by the weighted sum:

$$z_\sigma = \frac{\sum_{V_\sigma} |\rho| z}{\sum_{V_\sigma} |\rho|} \quad (4)$$

where  $V_\sigma$  denotes the set of neighbour pixels that lie within a distance of  $\sigma$  m from the centre pixel and  $\rho$  is the complex degree of coherence. Parameter  $\sigma$  will be referred to as scale parameter since it influences the amount of smoothing of the original  $z$ -coordinate. By weighing with coherence magnitude, more weight is given to neighbourhood pixels with a better defined scattering phase center. Low coherence can be due to radar shadow, where, due to thermal noise, the phase difference has larger variation and the coherence decreases. Another reason for low coherence is lay-over, where different scattering heights contribute to the same pixel. In both cases the interferometric  $z$ -coordinate is less well defined and will get a lower weight in the averaging. In the following sections different steps in the segmentation procedure will use filtered images with different values for the scale parameter. For instance the parameters  $\sigma_{\text{location}}$ ,  $\sigma_{\text{circle}}$ , and  $\sigma_{\text{Fourier}}$  will be introduced to indicate values for the scale parameter used in the different steps.

The filtered  $z$ -coordinate is now used to calculate the gradient image:

$$\nabla_{z_\sigma} = \left\langle \frac{\partial z_\sigma}{\partial x}, \frac{\partial z_\sigma}{\partial y} \right\rangle \quad (5)$$

where the derivatives are approximated by finite differences.

Worring et. al. 1996 were to our knowledge the first to use both gradient magnitude and gradient direction for optimizing a segment boundary. The boundary of a tree crown will be best approximated when, at all points on

the boundary, the gradient is maximum, and directed inwards, orthogonal to the boundary. For a certain point on the boundary, this means maximizing the dot product:

$$-\nabla_{z_\sigma} \cdot \frac{v'_\perp(t)}{|v'(t)|} \quad (6)$$

where the second term is a unit size outward pointing normal vector orthogonal to the boundary. This dot product can then be integrated along the boundary using a line integral with respect to curve length. For the total boundary the following function can be used:

$$f_\sigma(v) = -\frac{1}{s} \int_t -\nabla_{z_\sigma} \cdot \frac{v'_\perp(t)}{|v'(t)|} \cdot |v'(t)| dt \quad (7)$$

where the factor  $1/s$  has been introduced to make the function independent of the total curve length. Tree crown image segmentation can now be posed as an optimization problem; find the local maximum of  $f_\sigma$  in the neighbourhood of initial guess.

### 4.2 Selection of candidate segment locations

For an operational monitoring system we need to limit the number of function evaluations. We therefore select candidate segment locations  $a_{\text{init}}, c_{\text{init}}$  that are likely to generate valid tree crown segments. The question whether a segment is the 2D radar projection of a physically feasible tree crown (the recognition problem) is postponed until after the segmentation and is not treated in this paper. However, a natural candidate for deciding whether a segment represents a real tree crown is  $f_\sigma$  since it is a measure of the gradient magnitude along the boundary. For now, local maxima in the filtered  $z$ -coordinate are identified as candidate segment location. The procedure is as follows. First, a filtered  $z$ -coordinate image  $\sigma_{\text{location}}=6$  m is calculated. Secondly, all pixels that are local maxima in the filtered image are determined. Thirdly, only those maxima that have no other maxima with a larger value within a distance of 6 m are identified as candidate segment locations. The procedure depends on a single parameter: scale parameter  $\sigma_{\text{location}}$ . A small value results in a large number of candidate locations whereas a large value results in a small number of candidate start locations.

### 4.3 Search strategy

In the previous subsection we explained how a set of candidate boundary locations was derived. The boundary translation parameters are initialized with these candidate locations. We also need initial values for the other parameters. We have found that a good initial shape is a circle with radius 8 m corresponding to the average crown size of large trees. The rotation angles and the relative phase of the second ellipse are initially set to zero. Instead of trying to optimize the values of all parameters simultaneously we divide them in groups. First we optimize the translation and size of

the circle. The optimum values found:  $a_{\text{circle}}$ ,  $c_{\text{circle}}$  and circle radius are then used as initial values for a second and final search. In the final search all Fourier parameters are allowed to change. In both optimization searches Powell's direction set method is used (Press et. al. 1994) to find the optimum parameter values.

There is another distinction between the two searches. For finding the optimal circle we use a large scale parameter  $\sigma = \sigma_{\text{circle}}$  to calculate the weighted  $z$ -coordinate image and the corresponding gradient image. For  $\sigma_{\text{circle}}$  we have found empirically that a value close to 5 m gives good results. In the results section we demonstrate the sensitivity of the resultant boundary to the parameter  $\sigma_{\text{circle}}$ . Scale parameter  $\sigma_{\text{circle}}$  is essentially a fit parameter for the procedure and could be optimized when accurate ground truth information is available. Using such a large smoothing initially prevents the boundary to become trapped in a local optimum too soon in the optimization procedure. In the second and final search we use a gradient image with  $\sigma = \sigma_{\text{Fourier}}$ . The value for  $\sigma_{\text{Fourier}}$  is always smaller than the value for  $\sigma_{\text{circle}}$  allowing more accurate positioning of the boundary. The shape can then adjust to irregular shaped tree crowns. A typical value for  $\sigma_{\text{Fourier}}$  that performs well for finding the final Fourier parameters is 2 m. (We have found that due to noise some smoothing is always required, even in the final stage of the algorithm).

The search strategy can now be summarized in the following four steps:

1. Initialize circular boundary with radius 8 m and location  $a_{\text{init}}, c_{\text{init}}$ .
2. Use Powell's direction set method to optimize the circle position radius using a gradient image generated with the scale parameter set to 5 m.
3. Initialize the Fourier boundary ( $K=3$  harmonics) with best circle
4. Use Powell's direction set method to optimize the Fourier boundary parameters using a gradient image with the scale parameter set to 2 m.

### 5 Calculation of the 3D crown position

The  $z$ -coordinate of a pixel is calculated from the phase difference and the known interferometer geometry as (Goblirsch, 1997):

$$z = H + C \frac{B_z}{2} - \frac{B_y}{2} \sqrt{\frac{4r^2}{B_y^2 + B_z^2} - C^2} \quad (8)$$

where

$$C = 1 - \frac{\left(\frac{\phi\lambda}{4\pi}\right)^2 + 2r\left(\frac{\phi\lambda}{4\pi}\right)}{B_y^2 + B_z^2} \quad (9)$$

with  $\phi$  the phase difference,  $r$  the range distance to the pixel,  $H$  the aircraft altitude,  $B_y, B_z$  the horizontal and vertical baseline components respectively, and  $\lambda$  the wavelength. The  $y$ -coordinate of a pixel is now obtained with

$$y = \sqrt{r^2 - (H - z)^2} \quad (10)$$

The  $x$ -coordinate follows from the azimuth pixel spacing. It is assumed that at C-band, scattering from vegetation results in a bivariate complex Gaussian random variable for the observed complex signal. See Goodman (1963) and Goodman (1985) for a derivation of this Gaussian model. Averaging (or multi-looking) is often applied for SAR data reduction. In this paper we are interested in the marginal probability density function (pdf) of the multi-look phase difference. An expression for this density function was given by Tough et. al. (1995). Since the  $y$ -, and  $z$ -coordinate follow from the interferometric phase difference, they must be treated as random variables. Given the number of independent looks, a 95% confidence interval can be constructed for the  $y$ -, and  $z$ -coordinate using the multi-look phase difference pdf. Figure 3 shows the one sided 95% confidence level as a function of the coherence magnitude and the number of independent looks.

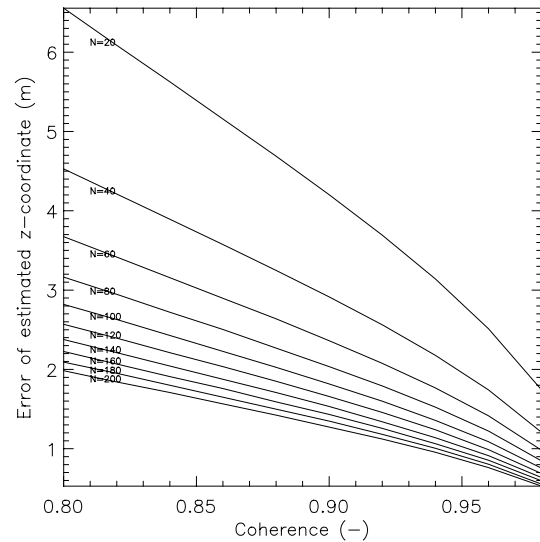


Figure 3. Error of estimated  $z$ -coordinate as a function of the coherence and the number of looks. Calculations were done using the following parameter values: reference height  $z=0$  m. SAR altitude  $H=3237$  m; interferometric baseline  $B_y=0.23$  m,  $B_z=0.93$  m; range  $r=6307$  m.

The figure shows that approximately 100 independent looks need to be averaged to decrease the error to less than 3 m. To determine the effective number of independent looks, the coherence of a river water surface in the far range was measured and compared with theoretical average values given in (Touzi et. al. 1999). We estimated that the independent number of

looks was at least 4 looks per pixel. In order to estimate the crown position within 3 m accuracy we would therefore need at least 25 pixel per tree crown. However, a preliminary analysis has shown that pixels are significantly correlated which reduces the number of independent looks by a factor of 0.62.

After the crown  $y$ -, and  $z$ -coordinate are calculated from the phase difference, they need to be corrected because of the Van Cittert-Zernike Theorem. How this is done is the subject of another paper (Hoekman and Varekamp, 1998).

## 6 Results and Discussion

Figure 4 shows the effect of scale parameter  $\sigma_{\text{circle}}$  for nine different segments when optimizing the position and radius of a circle. For a value of  $\sigma_{\text{circle}} \geq 5$  m, the circle position and radius stay approximately. This indicates that the optimal circle when varying both radius and position is not very sensitive to the scale parameter. The circle approximation seems already a good fit for boundaries #1, #12 and #14.

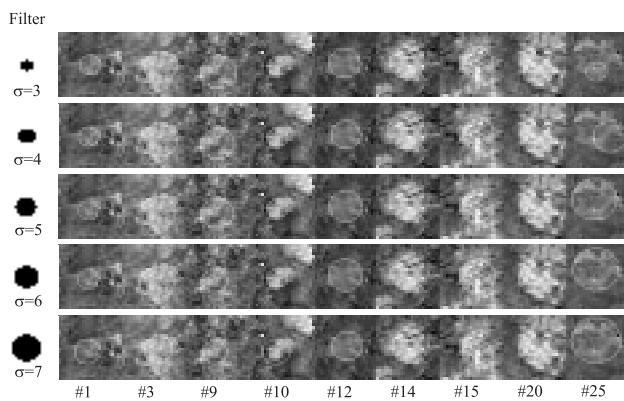


Figure 4. Effect of scale parameter  $\sigma_{\text{circle}}$  for nine different segments for  $\sigma_{\text{position}} = 6$ .

Figure 5 shows the Fourier segmentations. As can be seen, Fourier boundaries fit better than the circles. This is especially evident for boundaries #1, #3, #9, #10, #14 and #25.



Figure 5. Fourier segmentations for  $K=3$  harmonics,  $\sigma_{\text{position}} = 6$ ,  $\sigma_{\text{circle}} = 5$  and  $\sigma_{\text{Fourier}} = 2$ .

Figure 6 presents an ortho-projection of the boundaries in ground range radar coordinates. Circular boundaries are displayed with a yellow color and Fourier boundaries are displayed with a red color. The ground measurements are displayed in white. The tree crown surrounded by boundary #14 was used to register the ground data with the radar data. The grey scale background image of figure 6 was produced as follows. The  $y$ - and  $z$ -coordinate of each pixel were calculated. These coordinates were not corrected for displacements caused by lay-over. The  $x$ -coordinate of each pixel was calculated from the azimuth pixel spacing. Each pixel was then rendered separately as a horizontal flat plate in three-dimensional (3D) space. The background radar image of figure 6 is thus an ortho-projection of the flat plates as plotted in 3D space. Flat plates with a coherence of less than 0.5 are not shown. The brightness of each flat plate is proportional to the  $z$ -coordinate. The  $z$ -coordinate ranges between 85 m (black) and 195 m (white).

caused by lay-over. The  $x$ -coordinate of each pixel was calculated from the azimuth pixel spacing. Each pixel was then rendered separately as a horizontal flat plate in three-dimensional (3D) space. The background image of figure 6 is thus an ortho-projection of the flat plates as plotted in 3D space. Flat plates with a coherence of less than 0.5 are not shown. The brightness of each flat plate is proportional to the  $z$ -coordinate. It can be seen some areas are more populated with flat plates than other areas. Also, sometimes very high values occur in areas where other pixels have low value. These flat plates have a low coherence close to 0.5 and their location is thus rather inaccurate.

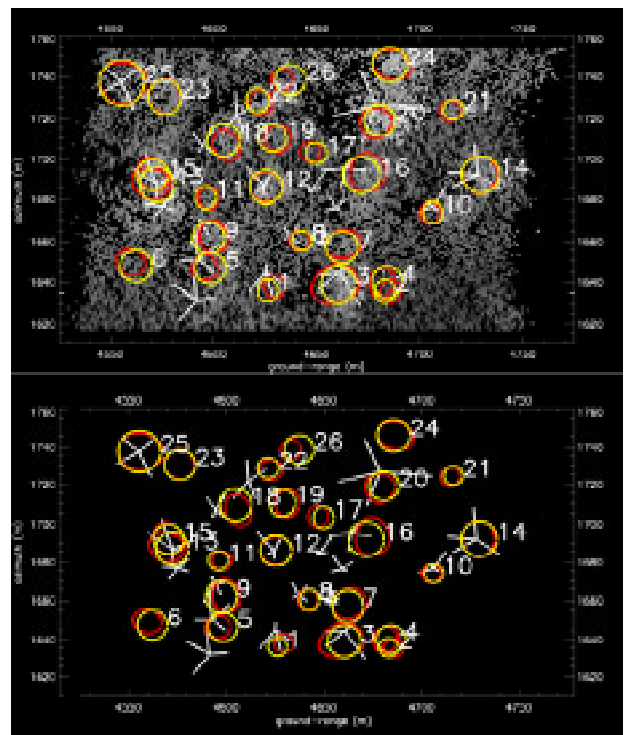


Figure 6. Ortho-projection of the boundaries in ground range radar coordinates. The top image gives the boundaries on top of a radar image. The bottom image gives the boundaries on a black background. Circular boundaries have a yellow color, Fourier boundaries have a red color. The ground measurements are displayed in white. The tree crown surrounded by boundary #14 was used to register the ground data with the radar data. The grey scale background image was produced as follows. The  $y$ - and  $z$ -coordinate of each pixel was calculated. These coordinates were not corrected for displacements caused by lay-over. The  $x$ -coordinate of each pixel was calculated from the azimuth pixel spacing. Each pixel was then rendered separately as a horizontal flat plate in three-dimensional (3D) space. The background radar image of figure 6 is thus an ortho-projection of the flat plates as plotted in 3D space. Flat plates with a coherence of less than 0.5 are not shown. The brightness of each flat plate is proportional to the  $z$ -coordinate. The  $z$ -coordinate ranges between 85 m (black) and 195 m (white).

Boundaries lie within 5 m distance from the true tree trunks in most cases. The relationship between boundary size and the true ortho-projection of the tree crown is not so strong. Only boundaries #12 and #25

seem to give estimates with an error of less than 5 m. A possible explanation is that shadow regions often border lay-over regions. Both shadow regions and lay-over regions have low coherence and thus a high noise level which makes boundary placement inaccurate.

## 7 Conclusions

We have shown that the  $z$ -coordinate as calculated from measurements with an airborne interferometric SAR system can be segmented successfully when gradient information is used together with a Fourier parameterization for the 2D radar-projection of a tree crown. Limiting the number of Fourier harmonics to  $K=3$  seems appropriate for representing the boundary. Current ground data sets are not suitable for obtaining detection statistics such as the percentage of tree crowns detected and the number of false alarms. Better ground data sets will be needed in future to evaluate algorithm performance for real tree mapping situations.

## Acknowledgements

The Netherlands Remote Sensing Board and the Netherlands Ministry of Economic Affairs are acknowledged for financial support. Emile Hendriks and Marcel Reinders (Faculty of Electrical Engineering, Delft University of Technology) are acknowledged for their suggestions concerning deformable models.

## References

- Bamler, R., and Hartl, P., 1998, Synthetic Aperture Radar Interferometry. *Inverse Problems*, **14**, 1-54.
- Chakraborty, A., and Duncan, J.S., 1999, Game-Theoretic Integration for Image Segmentation. *IEEE Transactions on Pattern Analysis and Machine Intelligence*, **21**, 12-30.
- Cootes, T.F., Taylor, C.J., Cooper, D.H., and Graham, J., 1995, Active Shape Models - Their Training and Application. *Computer Vision and Image Understanding*, **61**, 38-59.
- Edwards, C.H., and Penney, D.E., 1994, *Calculus with Analytic Geometry* (London: Prentice Hall).
- Faller, N.P., 1998, Operational Topographic Mapping in Indonesia with the Interferometric DO-SAR. In *Proceedings of the European Conference on Synthetic Aperture Radar (EUSAR'98)*, Friedrichshafen, Germany, 25-27 May 1998, pp. 439-443 (Berlin: ITG/VDE).
- Goblirsch, W., 1997, Optimization of Geometric Parameters for Interferometric Surface Model Generation. *Ph.D. Thesis*, University Zürich.
- Goodman, J., 1985, *Statistical Optics*, (New York: Wiley-Interscience).
- Goodman, N.R., 1963, Statistical Analysis Based on a Certain Multivariate Gaussian Distribution (an Introduction). *The Annals of Mathematical Statistics*, **34**, 152-177.
- Hoekman, D.H., and Varekamp, C., 1998, High Resolution Single-Pass Interferometric Radar Observation of Tropical Rain Forest Trees. In *Proceedings of the Second International Workshop on Retrieval of Bio- and Geo-Physical Parameters from SAR Data for Land Applications*, ESTEC, Noordwijk, The Netherlands, 21-23 October 1998, pp. 233-239.
- Kass, M., Witkin, A., and Terzopoulos, D., 1988, Snakes: Active Contour Models. *International Journal of Computer Vision*, **1**, 321-331.
- Press, W.H., Teukolsky, S.A., Vetterling, W.T., and Flannery, B.P., 1994, *Numerical Recipes in C: The Art of Scientific Computing*. 2nd edn (Cambridge: Cambridge University Press).
- Staib, L.H., and Duncan, J.S., 1992, Boundary Finding with Parametrically Deformable Models. *IEEE Transactions on Pattern Analysis and Machine Intelligence*, **14**, 1061-1075.
- Tough, R.J.A., Blacknell, D., and Quegan, S., 1995, A Statistical Description of Polarimetric and Interferometric Synthetic Aperture Radar Data. *Proceedings of the Royal Society of London A*, **449**, 567-589.
- Touzi, R., Lopes, A., Bruniquel, J., and Vachon, P.W., 1999, Coherence Estimation for SAR Imagery. *IEEE Transactions on Geoscience and Remote Sensing*, **37**, 135-149.
- Wooding, M.G., Zmuda, A.D., Hoekman, D.H., de Jong, J.J., and Attema, E., 1999, The Indonesian Radar Experiment (INDREX-96). *Earth Observation Quarterly*, **61**, 23-29.
- Worring, W., Smeulders, A.W.M., Staib, L.H., and Duncan, J.S., 1996, Parameterized Feasible Boundaries in Gradient Vector Fields. *Computer Vision and Image Understanding*, **63**, 135-144.